

COMMUNICATION

Cryo-trapping the Six-coordinate, Distorted-octahedral Active Site of Manganese Superoxide DismutaseGloria E. O. Borgstahl^{1*}, Matthew Pokross¹, Ramsey Chehab¹, Anuradha Sekher¹ and Edward H. Snell²¹*Department of Chemistry, The University of Toledo, 2801 West Bancroft Street, Toledo OH 43606, USA*²*NASA, Laboratory of Structural Biology, Code SD48 Marshall Space Flight Center Huntsville, AL 35812, USA*

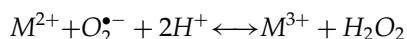
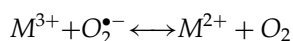
Superoxide dismutase protects organisms from potentially damaging oxygen radicals by catalyzing the disproportionation of superoxide to oxygen and hydrogen peroxide. We report the use of cryogenic temperatures to kinetically capture the sixth ligand bound to the active site of manganese superoxide dismutase (MnSOD). Synchrotron X-ray diffraction data was collected from *Escherichia coli* MnSOD crystals grown at pH 8.5 and cryocooled to 100 K. Structural refinement to 1.55 Å resolution and close inspection of the active site revealed electron density for a sixth ligand that was interpreted to be a hydroxide ligand. The six-coordinate, distorted-octahedral geometry assumed during inhibition by hydroxide is compared to the room temperature, five-coordinate, trigonal bipyramidal active site determined with crystals grown from practically identical conditions. The gateway residues Tyr34, His30 and a tightly bound water molecule are implicated in closing-off the active site and blocking the escape route of the sixth ligand.

© 2000 Academic Press

Keywords: manganese; superoxide dismutase; cryocrystallography; solvent structure; metalloprotein

*Corresponding author

Superoxide dismutases (SODs) are important antioxidant enzymes that protect all living cells against toxic oxygen metabolites. SOD catalyzes the dismutation of superoxide to oxygen and hydrogen peroxide, utilizing a reaction mechanism that involves the cyclic oxidation and reduction of the active site metal ion coupled to the protonation of the coordinated anion (Holm *et al.*, 1996).



SODs are some of the fastest known enzymes and are rate-limited only by the diffusion of their small substrate and products (Bannister *et al.*, 1987). SODs contain Cu/Zn, Fe or Mn ions in their active sites. FeSOD is found only in bacteria, whereas MnSOD is found only in mitochondria. In fact, defects in human MnSOD have been implicated in several late-onset diseases associated with aging.

Most crystal structures of MnSOD have been determined at room temperature and have a five-

coordinate, trigonal bipyramidal active site geometry (Figure 1) (Ludwig *et al.*, 1991; Borgstahl *et al.*, 1992; Edwards *et al.*, 1998b). Two cryocooled crystal structures of MnSOD have been determined to date. The cryogenic 2.3 Å resolution structure of Q143N mutant human MnSOD had a five-coordinate active site manganese ion (Hsieh *et al.*, 1998). The cryogenic 2.2 Å resolution structure of an iron-substituted MnSOD had one subunit metal atom that was five-coordinate and the other subunit metal atom was six-coordinate (Edwards *et al.*, 1998a). This difference in coordination state from the five-coordinate native MnSOD was attributed to the metal substitution. A six-coordinate manganese active site was seen in the room temperature 1.8 Å resolution azide complex of *Thermus thermophilus* MnSOD (Lah *et al.*, 1995). Here, we report the 100 K, 1.55 Å resolution structure of *Escherichia coli* MnSOD, the highest-resolution MnSOD structure reported to date. Through cryocooling, the rapidly exchanged sixth ligand has been trapped in a distorted-octahedral manganese active site.

In modern crystallography, cryogenic temperatures are frequently used in combination with synchrotron radiation to reduce radiation damage and to extend diffraction resolution. Cryocrystallogra-

E-mail address of the corresponding author: gborgst@uoft02.utoledo.edu

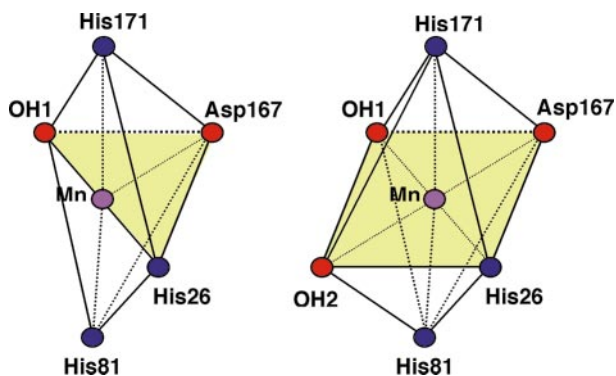


Figure 1. Diagrams of the five-coordinate trigonal bipyramidal and six-coordinate octahedral active sites of *E. coli* MnSOD. For overproduction of MnSOD, the *E. coli* strain OX326A.1 (pTTQA10) was used. This strain lacks endogenous Mn and FeSODs and harbors an ampicillin-resistant, IPTG-inducible expression plasmid for *E. coli* MnSOD (Hopkin *et al.*, 1992; Steinman, 1992). Bacterial cultures were grown at 37°C in four liters of Terrific Broth supplemented with 4 mg MnSO₄ and 200 mg ampicillin in a VRTI-culture fermentor (10 l O₂/minute, 300 RPM). At mid-log stage the culture was induced with 1 mM IPTG. After four hours, cells were harvested, resuspended in 50 mM potassium phosphate (pH 7.5), lysed by sonication and centrifuged. The following rapid purification protocol was adapted from published procedures (Beck *et al.*, 1988; Borgstahl *et al.*, 1992; Keele *et al.*, 1970). The clarified lysate was heated to 60°C for one hour and centrifuged. The supernatant was then dialyzed against 5 mM potassium phosphate (pH 7.5), mixed with preequilibrated DE-52 resin and incubated for one hour. The filtrate was then dialyzed against 2.5 mM MES (pH 5.5) and applied to a PerSeptive BioSystems CM/M POROS[®] column. The column was thoroughly washed and eluted with a gradient of 2.5 mM to 500 mM MES (pH 5.5). Very pure MnSOD eluted at approximately 200 mM MES. Peak fractions were pooled and dialyzed against 20 mM potassium phosphate (pH 7.0). Approximately 15–20 mg of MnSOD was purified per liter of culture. Activity was monitored with a qualitative native polyacrylamide gel electrophoresis based assay stained with *p*-nitroblue tetrazolium (Calbiochem). Protein samples were concentrated to 20 mg/ml and crystallized by the vapor diffusion method using sitting drops containing 2 µl of protein at 15 mg/ml plus 2 µl of reservoir solution. Drops were equilibrated over 500 µl of reservoir solution and crystals appeared in seven days. A long single crystal was grown from 50 mM bicine (pH 8.5) and 25% PEG 6000. This crystal was square in cross section (200 µm × 200 µm), over 1 mm long and was cut into several pieces each approximately 250 µm long. Pieces 2 and 3 were cryocooled and diffraction data collected at SSRL beamline 7-1 for structure determination. The structure was determined using data from piece 3. Piece 1 was mounted in a capillary and room temperature crystal mosaicity measurements were taken at SSRL beamline 1-5 in unfocussed mode using super-fine ϕ slicing the following day. Mosaicity values of the order of 0.008° were measured.

phy has been used to trap reaction intermediates, since lowering the temperature can slow enzymatic

reactions and limit the movements of the protein and the solvent. For example, the first intermediate in the photocycle of photoactive yellow protein was determined to 0.85 Å resolution by stimulating cryocooled crystals with light (Genick *et al.*, 1998). In addition, the photodissociation of carbon monoxide from myoglobin was studied using cryocrystallography (Schlichting *et al.*, 1994). We therefore postulated that cryocooling would slow the dissociation kinetics of the sixth ligand in the MnSOD active site enough to allow for an atomic picture of its structure to be captured.

From a variety of experimental data on native and inhibited SOD, two different reaction mechanisms have been proposed for Mn and FeSODs. The first reaction mechanism, called 5-6-5, was proposed on the basis of crystal structure analysis and X-ray absorption studies (Lah *et al.*, 1995; Ludwig *et al.*, 1991; Tierney *et al.*, 1995). These researchers conclude that the anions that inhibit SOD (e.g. azide, fluoride and hydroxide) bind in the same way as the superoxide anion. Several structures of *E. coli* FeSOD and *T. Thermophilus* MnSOD have been determined at 1.8 Å resolution. Native structures were five-coordinate and azide complexes had a 6-coordinate distorted-octahedral active site manganese ion (Lah *et al.*, 1995). Cryogenic X-ray absorption spectroscopy of the iron site in FeSOD indicated that at neutral pH the iron atom is five-coordinate, at pH 10.5 it is six-coordinate and at pH 9.4 there is a 1:1 mixture of the two states (Tierney *et al.*, 1995). It was presumed that the sixth ligand was hydroxide. In the 5-6-5 mechanism proposed from these studies, the metal is five-coordinate in its resting state and six-coordinate when anion is bound (Lah *et al.*, 1995).

Studies on the temperature-dependent absorption or thermochromism of anion complexes of *E. coli* MnSOD led to a second proposal for the reaction mechanism, called associative-displacement (Whittaker & Whittaker, 1996). Room temperature optical absorption spectra for native MnSOD at pH 7.0 and anionic inhibitors (azide and fluoride) indicated five-coordination. In the presence of inhibitors, the active site structure was altered and the spectra of the anionic complexes were characteristic of six-coordination at low temperature with a midpoint for the transition near 200 K. Interestingly, for MnSOD in the absence of added anions the spectra represented five-coordinate metal throughout the temperature range studied. In the resulting associative-displacement mechanism, it is proposed that the anionic inhibitors result in an inactive form of the enzyme and that in the active form of the enzyme the active site metal is always five-coordinate, with anion binding displacing one of the manganese ligands.

The experimental data in the above studies on Mn and FeSOD agree, although their interpretation and the reaction mechanisms proposed do not. Both studies show that when sufficient quantities of anionic inhibitor are present, cryogenic conditions can promote the octahedral state of the

Table 1. Data collection and space group statistics

Beamline		SSRL 7-1	
Detector		MAR345	
Temperature (K)		100	
Wavelength (Å)		1.08	
Spacegroup		C222 ₁	
Unit cell dimensions (Å)		$a=99.11, b=107.30, c=179.11$	
No. monomers in asymmetric unit		4	
Matthews coefficient, V_M (Å ³ /Da)		2.59 (54.1%, v/v, solvent)	
X-ray data	High-resolution	Low-resolution	Combined
Number of Images	66	45	
Approximate exposure time (s)	40	10	
Oscillation angle, $\Delta\phi$ (deg.)	1.5	2	
Crystal to detector distance (mm)	200	250	
Resolution range (Å)	4.0-1.55	26.0-2.44	26.0-1.55
Number of observations	670,699	177,625	848,324
Unique reflections	na	na	135,855
Completeness (%)	na	na	98.8 (98.8)
$I > 3\sigma(I)$	na	na	83.5 (61.1)
Mean $I/\sigma(I)$	na	na	6.5(3.0)
Multiplicity	na	na	4.2 (3.1)
R_{sym} (%)	na	na	7.0 (24.1)

Synchrotron data were collected in dose mode and the corresponding time in seconds is given. The entire data set took four hours to collect. The X-ray data were processed using MOSFLM 6.0 (Leslie, 1990) and programs from the CCP4 package (1994). Solvent content calculations were based on the expected solvent content of protein crystals (Matthews, 1968). $R_{\text{sym}} = \sum_{hkl} (|I_{hkl}| - I_{hkl}) / \sum_{hkl} I_{hkl}$. Statistics from the 1.55-1.62 Å shell are in parentheses. na, not applicable (these statistics were obtained after scaling the combined data).

enzyme. In the absence of inhibitor or natural ligand, the active site metal atom remains five-coordinate when cryocooled. The proposed mechanisms could be tested by capturing the elusive ligation intermediates of MnSOD through cryocooling, envisioning the active site structures with crystallography, and counting the number of ligands in the active site. This is the first of such studies.

Cryogenic structure determination

It is thought that small molecules coordinate to both the oxidized and reduced metal centers in MnSOD (Whittaker & Whittaker, 1991) and in this study MnSOD was purified and crystallized in the redox heterogeneous form. Crystals of MnSOD were grown from alkaline solutions of phosphate, and PEG 6000. MnSOD crystals of space group C222₁ have been shown to be active (Whittaker *et al.*, 1998). For cryogenic data collection, a 250 µm long piece of the crystal grown from PEG 6000 at pH 8.5 was soaked in reservoir solution plus 20% (v/v) glycerol and cryocooled to 100 K using a nitrogen gas stream. Diffraction to 1.3 Å resolution was recorded but only data to 1.55 Å resolution could be resolved due to the long c axis of the unit cell (Table 1) and the physical limitations of the instrumentation. Based on the measured unit cell dimensions, the Matthews coefficient (V_M) indicates that there are two homodimers in the asymmetric unit, giving four atomic views of the manganese-containing active site.

Edwards *et al.* (1998b) determined the first structure of *E. coli* MnSOD at 2.1 Å resolution from room temperature crystals that are isomorphous with the crystals used in this study. Molecular replacement was performed by using the room

temperature structure (PDB code 1 VEW) for starting coordinates followed by rigid body, positional and B -value crystallographic refinement (Brunger, 1992). Completely new solvent structure and the active site manganese ions with their covalently bound protein and hydroxyl ligands were modelled during the last stages of refinement (Table 2). Omit $F_o - F_c$ electron density maps for the refined model exhibited excellent density for the entire main-chain of each subunit and good density for most side-chains. Due to cryocooling, the protein atoms have low atomic mobility with B -values ranging from 2.0 to 44.5 Å², with an average value of 13.4 Å². Water molecule B -values ranged from 6.0 to 61.7 Å², with an average value of 28.2 Å². The active sites were very well ordered, with average B -values of 6.9 and 8.0 for the manganese and bound hydroxide, respectively. The stereochemical agreement with ideality for bond lengths and angles was excellent. Analysis by PROCHECK indicates that 91.7% and 7.2% of residues fall within the sterically most favored regions and additional allowed regions of a Ramachandran plot, respectively (Laskowski *et al.*, 1993). In all subunits, residues Asn145 and Gln178 have normally disallowed ϕ and ψ angles and are at the second position of type II' turns.

Description of structure

The *E. coli* MnSOD monomer fold and dimer interface have been described in detail (Edwards *et al.*, 1998b) and will be summarized here briefly. The tertiary structure is very similar to that described for other Fe and MnSODs (Ludwig *et al.*, 1991; Borgstahl *et al.*, 1992; Lah *et al.*, 1995). *E. coli* MnSOD functions as a homodimer (Figure 2(a)) with the pink active site manganese atoms separ-

Table 2. Refinement statistics

A. Contents of model	
Protein	4×205 amino acid residues
Dual conformers	21
Manganese	4
Hydroxide ligands	8
Solvent molecules	1093
B. Geometry	
r.m.s.d. bonds (Å)	0.005
r.m.s.d. angles (deg.)	1.210
C. X-ray data (%)	
R-factor (20–1.55 Å)	19.4
Free R-factor (20–1.55 Å)	23.3
D. Average B-factors (Å ²)	
Protein	13.5 (s.d. 5.88)
Manganese	6.91 (s.d. 0.30)
Hydroxide ligands	
OH1	7.8 (s.d. 1.35)
OH2	8.7 (s.d. 1.35)
Solvent	28.2 (s.d. 12.2)

Refinement was performed using X-PLOR 3.851 (Brunger, 1992). The 2.1 Å structure of *E. coli* MnSOD (1VEW) was used as a starting model (Edwards *et al.*, 1998b). All water molecules, dual conformers and manganese atoms were omitted and the initial *R* value was 49.5% ($R_{\text{free}} = 50\%$) for data greater than 2σ and between 20 and 4 Å resolution. Rigid body refinement reduced the *R* value to 33.6% ($R_{\text{free}} = 32.8\%$). Data to 3 Å resolution were introduced by positional refinement and then simulated annealing refinement reduced the *R* value to 27% ($R_{\text{free}} = 39.4$). The model was then subjected to positional and *B*-value refinement with data to 2.0 Å resolution ($R = 29.3$, $R_{\text{free}} = 35.7\%$). At this point the four Mn(III) atoms were modelled in the active sites and the bulk solvent correction was applied (density level $0.3495 \text{ e}^-/\text{Å}^3$ and *B* factor 85.4744 Å^2). Data were added to 1.55 Å resolution, water molecules with $F_o - F_c$ electron density greater than 3σ , and residues exhibiting dual conformations were modelled. Residues Ser6A, Glu54A, Thr69A, Ser122A, Lys134A, Lys186A, Ser6B, Glu47B, Glu55B, Asp61B, Ser122B, Asp136B, Lys20C, Lys29C, Ser122C, Glu54D, Glu55D, and Lys68D were modelled as dual conformers. The *WA* value recommended by CHECK was used for all refinement cycles. Active site Mn bond lengths were restrained to 2.2 Å for His and OH ligands and restrained to 2.0 Å for Asp (force constant 500). During the last cycles of the fifth ligand, OH1, was modelled and refined. Active site $F_o - F_c$ and omit $F_o - F_c$ maps (see Figure 3) were studied and a sixth ligand (OH2) was modelled and refined. The last stage of refinement included more *B*-value refinement and positional refinement with the relaxation of bond length restraints in the active site (force constant 10).

ated by 18.3 Å. Each monomer (Figure 2(b)) is composed of two domains: the N-terminal α -helical domain and the C-terminal α/β domain. The active site is nestled between the two domains with each domain contributing ligands to the active site coordination. Residues His26 and His81 from the N-terminal domain and Asp167 and His171 from the C-terminal domain are covalently bound to the manganese ion (Figure 2(b)). Two hydroxide ions, called OH1 and OH2, are bound to the manganese ion. Gateway residues His30, Tyr34, Trp128, Gln146, and Trp169 neighbor ligands OH1 and OH2 (Figure 2(c)). Residue Glu170 (not shown) of one monomer stretches across the dimer interface, forms a hydrogen bond with His171 of the other monomer, and thereby links the two active sites.

Most of the features of the room temperature, 2.1 Å resolution structure were retained and have been determined at a higher level of accuracy in the 100 K, 1.55 Å resolution structure. The tertiary structure of the monomers is very similar between the room temperature and 100 K structures with r.m.s.d. of 0.25 Å for main-chain atoms and 0.60 Å for all atoms. The quaternary structures of the homodimers are also very similar, as indicated by r.m.s.d. of 0.36 Å for main-chain atoms and 0.65 Å for all atoms. At room temperature, 21 side-chains displayed poor electron density (Edwards *et al.*, 1998b). Many of these disordered residues were modeled with dual conformations in the 1.55 Å maps from cryocooled crystals.

Active site geometry

In the final omit electron density map (Figure 3(a)) the sixth ligand, OH2, had electron density at 3.3, 2.6, 3.4 and 2.7 σ in active sites A, B, C and D, respectively. In comparison, the fifth ligand, OH1, had electron density values of 8.9, 9.0, 8.4 and 8.8 σ , respectively. The lower level of electron density for OH2 relative to OH1 could be due to higher mobility or lower occupancy. With the occupancy set to 1.0, the *B*-values of OH2 for active sites A, B, C and D refined to values of 30.2, 32.2, 28.3 and 36.8 Å², respectively. These *B*-values correlate well with the relative levels of electron density. The occupancy of OH2 was then manually adjusted while performing *B*-value refinement and occupancy values refining with *B*-values 1 Å² greater than OH1 were retained (Table 2). Occupancy estimates of 0.32, 0.28, 0.43 and 0.20 were obtained for active sites A, B, C, and D, respectively. At cryogenic temperatures the later interpretation of the data is probably the most correct. This occupancy/*B*-value refinement indicated that if OH1 is 100% occupied then 20–43% of the active sites in the crystal have both OH1 and OH2 bound simultaneously at pH 8.5. This is in good agreement with X-ray absorption measurements made over a range of pH values, which measured 50% occupancy of the sixth hydroxide ligand at pH 9.4 (Tierney *et al.*, 1995).

Overall, the covalent bonds to the manganese ion are more uniform in the 100 K structure than the room temperature structure (Table 3). The hydroxide ligand OH2-Mn bond length is 0.2 Å longer than OH1-Mn bond. The OH2-Mn bond is also 0.2 Å longer than the azide-Mn bond (Lah *et al.*, 1995). The longer bond of OH2 to Mn reflects the transient nature of this ligand. There is no indication of broken or weakened bonds to the active site metal for the other ligands or any indication of dual conformations for these ligands in the active site. Therefore, rather than displacing the OH1 or Asp167 ligand as predicted by the associative-displacement mechanism, OH2 appears to bind in a position *trans* to Asp167.

If the geometry about the manganese ion had perfect octahedral coordination, then the ligating

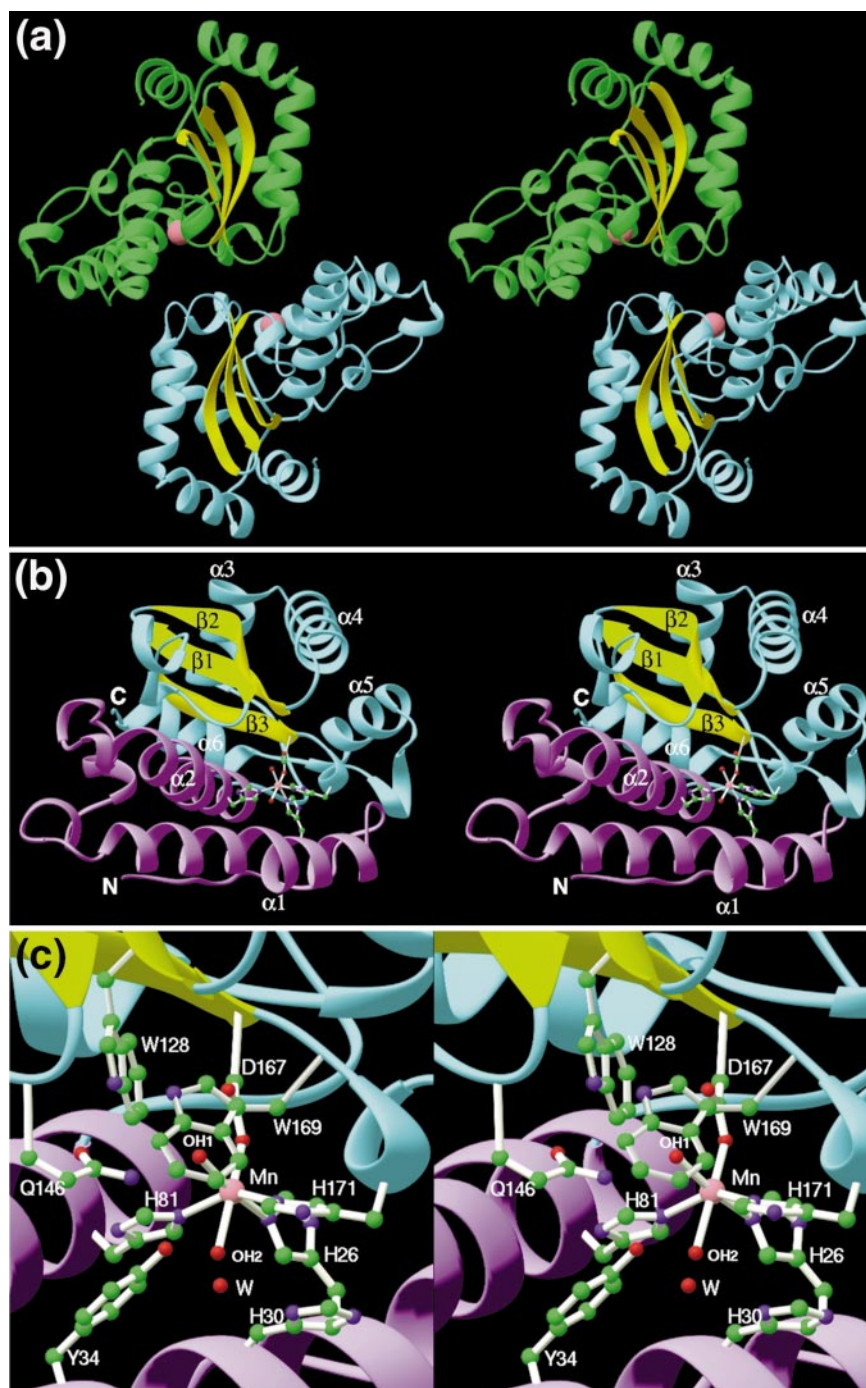


Figure 2. Stereopairs of ribbon diagrams of the MnSOD structure. (a) The homodimer; monomers are colored cyan and green, and the active site manganese atom is indicated with a pink sphere. (b) An individual monomer with pink manganese and six-coordinate active site. The N-terminal α -helical domain is colored purple and the C-terminal α/β domain is colored with cyan α -helices and yellow antiparallel β -pleated sheets. (c) Close-up view of the six-coordinate active site including the manganese ligands as well as the residues that neighbor the two hydroxide ligands.

atoms would be contained in three planes separated by 90° angles. In the 100 K MnSOD active site, the first plane containing atoms Mn, OH1, OH2, Asp167(O δ^2), and His26(N ϵ^2) and the second plane containing atoms Mn, OH2, His81(N ϵ^2), Asp167(O δ^2), and His171(N ϵ^2) are fairly planar (within 0.08 and 0.05 Å of a least-squares plane, respectively). The third plane, containing atoms

Mn, OH1, His26(N ϵ^2), His81(N ϵ^2), and His171(N ϵ^2), is distorted by 0.4 Å. Many of the active site bond angles are close to 90° (Table 3) but the angles between OH2(O)-Mn-His171(N ϵ^2) and OH2(O)-Mn-His81(N ϵ^2) are acute (73° and 67° , respectively) and the angles between His81(N ϵ^2)-Mn-Asp167(O δ^2) and His171(N ϵ^2)-Mn-Asp167(O δ^2) are obtuse (108° and 113° , respectively). Because the

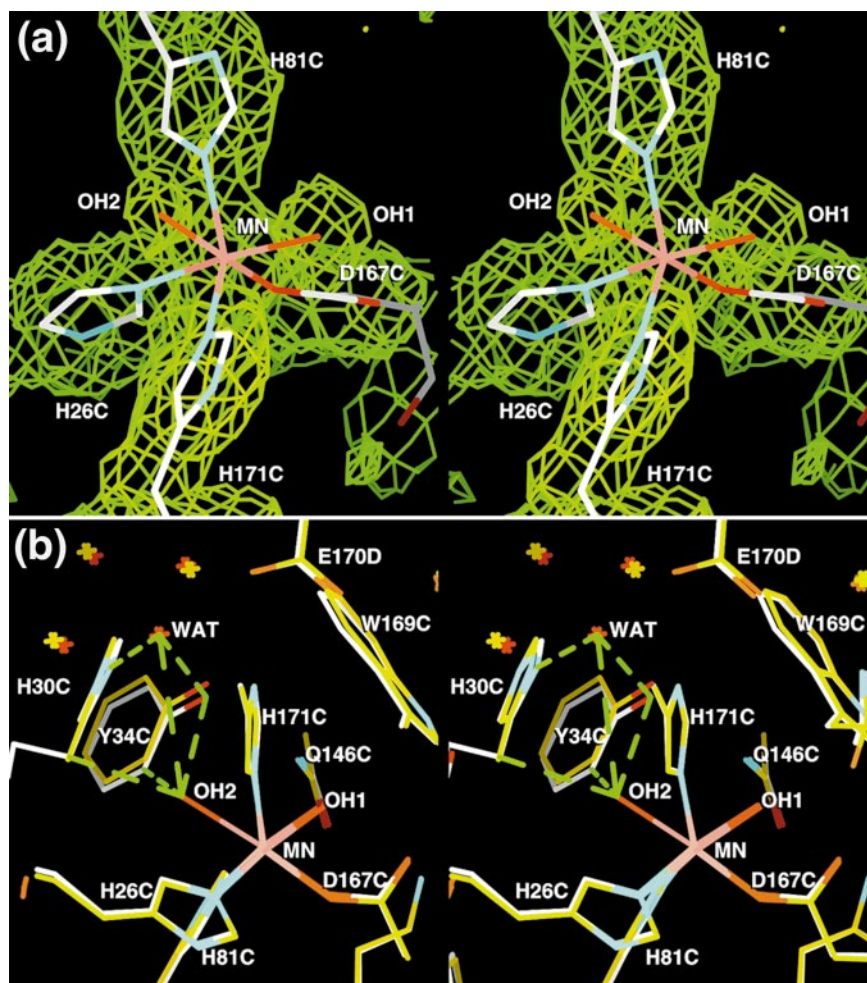


Figure 3. The six-coordinate, distorted octahedral manganese active site. (a) Omit electron density map for the active site of subunit C calculated with Fourier coefficients $F_o - F_c$ (2σ green contours) and phases derived from the final model with residues within a 4 Å sphere of the active sites omitted (183 omitted out of 7687 atoms). Positional refinement was performed after omission to remove phase bias. Atoms are colored: carbon, white; nitrogen, blue; oxygen, red; manganese, pink. (b) Superposition of room temperature (carbon and water yellow) onto the 100 K (carbon white, water red) MnSOD coordinates. The main-chain atoms of CD dimers were superimposed r.m.s.d. 0.35 Å and the active site of subunit C is illustrated. Hydrogen bonds between water (WAT) and His30 and Tyr34 as well as close contacts between OH2 and His30, Tyr34 and WAT are indicated with green broken lines.

angles between OH2(O)-Mn-His171(N^{ε2}) and OH2(O)-Mn-His81(N^{ε2}) are acute, there are close contacts between the rings of His81 and His171 and the sixth ligand OH2. These close contacts probably contribute to the fast off rate of the enzyme by pushing the reaction product away from the active site manganese by van der Waals repulsion. The active site bond angles of the room temperature and 100 K structure are very similar (Figure 3(b)). Close inspection of Table 3 shows that three of the active site bond angles were reduced significantly upon cooling (His26(N^{ε2})-Mn-Asp167(O^{δ2}), His26(N^ε)-Mn-His171(N^{ε2}), and His171(N^{ε2})-Mn-Asp167(O^{δ2}). Also, the His81(N^{ε2})-Mn-His171(N^{ε2}) angle opened 8.7° upon binding the OH2 ligand. The corresponding angle in *E. coli* FeSOD and *T. thermophilus* MnSOD opened 30° and 15°, respectively, upon binding azide at room temperature (Lah *et al.*, 1995).

Structural basis of cryotrapping

The positions of the gateway residues (Figure 2(c)) surrounding the two hydroxyl ligands are very similar in the room temperature and 100 K structure. The only significant differences are that the Tyr34(OH) and His30(N^{δ1}) move slightly closer (~0.5 Å to OH2 (Figure 3(b)). Analysis of neighbors within 4.0 Å of OH2 indicate that Tyr34, His30 and a water molecule hydrogen-bonded to Tyr34 hold the sixth ligand in place in the cryogenic state (Figure 3(b)). Atoms Tyr34(OH), Tyr34(C^{ε2}), His(C^β), and His(N^{δ1}) are 3.4, 3.1, 3.2 and 4.2 Å away from OH2, respectively. Under cryogenic conditions, His30 and Tyr34 side-chains have much lower thermal mobility with average side-chain *B*-values of only 9.7 Å² at 100 K and 24.6 Å² at room temperature. Many ordered solvent molecules fill the substrate funnel.

Table 3. Active site bond lengths, bond angles and hydrogen bond distances

	100 K	Room temperature
A. Covalent bonds (Å)		
Mn-His26(N ^{⊖2})	2.19(0.03)	2.14(0.04)
Mn-His81(N ^{⊖2})	2.19(0.02)	2.21(0.01)
Mn-Asp167(O ^{⊖2})	2.04(0.04)	2.02(0.01)
Mn-His171(N ^{⊖2})	2.19(0.01)	2.17(0.01)
Mn-OH1(O)	2.19(0.02)	2.21(0.05)
Mn-OH2(O)	2.42(0.01)	
B. Bond angles (deg.)		
OH2(O)-Mn-Asp167(O ^{⊖2})	176.4(7.2)	
OH1(O)-Mn-OH2(O)	92.6(3.7)	
OH2(O)-Mn-His26(N ^{⊖2})	95.4(3.4)	
OH2(O)-Mn-His171(N ^{⊖2})	72.6(5.8)	
OH2(O)-Mn-His81(N ^{⊖2})	66.9(3.6)	
OH1(O)-Mn-Asp167(O ^{⊖2})	85.3(0.5)	83.0(1.9)
OH1(O)-Mn-His171(N ^{⊖2})	90.4(1.5)	87.6(1.2)
OH1(O)-Mn-His81(N ^{⊖2})	93.1(2.7)	90.8(0.5)
His26(N ^{⊖2})-Mn-His81(N ^{⊖2})	93.2(1.6)	91.9(0.9)
His26(N ^{⊖2})-Mn-Asp167(O ^{⊖2})	87.0(0.7)	92.3(1.3)
His26(N ^{⊖2})-Mn-His171(N ^{⊖2})	88.9(1.5)	93.8(0.8)
His81(N ^{⊖2})-Mn-Asp167(O ^{⊖2})	108.0(2.4)	107.5(1.1)
His171(N ^{⊖2})-Mn-Asp167(O ^{⊖2})	112.7(1.6)	121.6(0.8)
His26(N ^{⊖2})-Mn-OH1(O)	173.4(4.4)	180.0(0.0)
His81(N ^{⊖2})-Mn-His171(N ^{⊖2})	138.8(3.6)	130.1(0.7)
C. Hydrogen bonds (Å)		
OH1(O)-Gln146(N ^{⊖2})	2.89(0.04)	2.90(0.08)
OH1(O)-Asp167(O ^{⊖1})	2.83(0.08)	2.78(0.04)
Gln146(N ^{⊖2})-Tyr34(OH)	2.94(0.02)	2.99(0.04)
Gln146(O ^{⊖1})-Asn80(N ^{⊖2})	3.25(0.08)	3.37(0.03)
Gln146(O ^{⊖1})-Trp128(N ^{⊖1})	2.97(0.01)	2.96(0.03)
D. Close contacts to OH2		
OH2(O)-His30(C [⊖])	3.22(0.13)	
OH2(O)-His30(N ^{⊖1})	4.17(0.20)	
OH2(O)-Tyr34(C ^{⊖2})	3.09(0.12)	
OH2(O)-Tyr34(OH)	3.43(0.23)	
OH2(O)-WAT	3.92(0.16)	

Average values were calculated over the four monomers in the asymmetric unit, standard deviations are enclosed by parentheses, and room temperature values were calculated from PDB entry 1VEW.

In particular, a water molecule hydrogen bonded to His30(N^{⊖1}) and Tyr34(OH) is only 3.9 Å from OH2. The water molecule firmly tethered between His30 and Tyr34 has average *B*-values of 25 Å². Subunits A and C in the room-temperature structure have no water modelled at this location (Figure 3(c)). In subunits B and D there are water molecules in similar locations but they are very weakly bound (*B*-values of 44 and 90 Å²) and are ~1 Å away from the 100 K water positions and in positions further away from the active site. The low *B*-values of the cryogenic structure reflect the rigidity of these residues. Therefore, the OH2 ligand is held in place by the neighboring residues Tyr34, His30 and the hydrogen bonded water. The tightly bound water molecule closes off the active site channel and prevents the escape of the sixth ligand.

Biological implications

We report the 1.55 Å structure of *E. coli* MnSOD at 100 K. The resolution of this structure determination is well within the covalent bond lengths of the active site ligands and therefore fairly accurate

bond lengths and bond angles have been obtained from unrestrained crystallographic refinement. At this temperature, the SOD protein and solvent become rigid and the anionic inhibitor bound to the sixth coordination site becomes trapped. This indicates that it is probably stereochemically possible to bind the sixth ligand at room temperature and that the only reason the sixth ligand has not been seen in electron density maps is that the kinetic rates of dissociation are too fast for it to be seen at room temperature.

Structures have been determined of both Fe and MnSODs with the inhibitor azide bound (Lah *et al.*, 1995). The 100 K MnSOD structure shows that both azide and hydroxide bind to the manganese ion in a position *trans* to Asp167. This binding site for hydroxide was seen also in the active site of FeSOD from *Propionibacterium shermanii* determined at room temperature and at 140 K (Schmidt, 1999). *P. shermanii* FeSOD is inhibited at much lower pH values than *E. coli* FeSOD, with inhibition starting at pH 6 in *P. shermanii* and pH 8 in *E. coli* (Bull & Fee, 1985). Several structures over a range of pH values were determined and all con-

tained with six-coordinate active sites. Notably, the 140 K structure of *P. shermanii* FeSOD at pH 8.1 showed higher occupancies for hydroxide in the sixth coordinate position than the room-temperature structure (occupancies increased from 0.36 to 0.46 for subunit A and from 0.10 to 0.38 for subunit B). All anionic inhibitors of Fe and MnSOD probably bind in this location. It is still unknown if the inhibitor-binding site is the same as the superoxide binding site or if the inhibitor-bound structure represents an inactive form of the enzyme.

The cryocooled, high-resolution picture of the distorted-octahedral intermediate of MnSOD included well-defined solvent structure. A role for gateway residues Tyr34, His30 and bound solvent in the reaction mechanism of MnSOD has been implicated. The water molecule that is tightly bound between Tyr34 and His30 caps off the MnSOD active site and prevents the release of hydroxide ligand. This shows the importance of accurate structural determination of the positions of solvent molecules in the understanding of the diffusion-limited reaction catalyzed by SOD.

Besides complexes with azide, why hasn't a six-coordinate active site been seen in previous MnSOD active sites? This is probably because most MnSOD structures to date have been determined at acidic or neutral pH and at room temperature. The five-coordinate, room-temperature structure of *E. coli* MnSOD had the same crystallization conditions as the 100 K structure. Apparently at room temperature, the hydroxide ligand was moving too fast to be seen in the crystals and cryocooling was required to slow the sixth hydroxide ligand enough for it to be visualized in electron density maps. The only other cryogenic structure of MnSOD to date was the Q143N mutant human MnSOD (Hsieh *et al.*, 1998). In these crystals, the pH was 4.6 and the active site was five-coordinate. Therefore, at neutral pH or lower the concentrations of hydroxide ion are insufficient for binding to be visualized.

If the binding of hydroxide mimics the binding of superoxide, our structure supports a 6-5-6-reaction mechanism (Lah *et al.*, 1995). The associative-displacement mechanism predicts that the bond to OH1 or Asp167 breaks and is displaced by the incoming ligand. There is no evidence of bond breaking or ligand displacement in the 100 K structure. Indeed, we have cryotrapped species number five (six-coordinate manganese with two hydroxide ligands) in the 6-5-6 reaction scheme.

The 100 K structure of MnSOD reported here demonstrates the utility of cryocrystallography to envision the structure of rapid reaction intermediates at high resolution. Caution should be exercised when comparing SOD structures obtained under conditions differing in pH and/or temperature (Edwards *et al.*, 1998a). Future studies include cryotrapping structures at higher alkalinity in order to obtain better occupancy of the sixth hydroxide ion. The underlying disagreement between the two reaction mechanisms of Mn and

FeSODs is whether anionic inhibitors bind in the same way as the natural substrate superoxide. One of the best ways to resolve this dilemma would be to solve the structure of SOD with superoxide bound. The 100 K structure of six-coordinate MnSOD reported here indicates that it may be possible to trap the superoxide anion binding to SOD using cryocrystallography. A tantalizing experiment would be to accumulate superoxide anions in MnSOD crystals prior to cryocooling and data collection.

Protein Data Bank accession code

The 1.55 Å resolution atomic coordinates of 100 K *E. coli* manganese superoxide dismutase have been deposited in the RCSB Protein Data Bank with ID code 1D5N.

Acknowledgments

We thank Dr Howard Steinman for kindly providing the expression plasmid and *sodAsodB* strain of *E. coli*, Dr Henry Bellamy for advice during data collection, and Dr Ewa Skrzypczak-Jankun and Krishnamurthy Rajeswari for technical assistance. E.H.S. is an NRC resident research associate at NASA(MSFC). This work has been supported financially by NASA grant NAG8-1380 to G.E.O.B. and E.H.S.

References

- Collaborative Computational Project No. 4 (1994). The CCP4 suite: programs for protein crystallography. *Acta Crystallog sect. D*, **50**, 760-767.
- Bannister, J. V., Bannister, W. H. & Rotilio, G. (1987). Aspects of the structure, function and applications of superoxide dismutase. *CRC Crit. Rev. Biochem.* **22**, 111-180.
- Beck, Y., Bartfeld, D., Yavin, Z., Levanon, A., Gorecki, M. & Hartman, J. R. (1988). Efficient production of active human manganese superoxide dismutase in *Escherichia coli*. *Bio/Technology*, **6**, 930-935.
- Borgstahl, G. E. O., Parge, H. E., Hickey, M. J., Beyer, W. F., Hallewell, R. A. & Tainer, J. A. (1992). The structure of human manganese superoxide dismutase reveals a novel tetrameric interface of two 4-helix bundles. *Cell*, **71**, 107-118.
- Borgstahl, G. E. O., Parge, H. E., Hickey, M. J., Johnson, M. J., Boissinot, M., Hallewell, R. A., Lepock, J. R., Cabelli, D. E. & Tainer, J. A. (1996). Human mitochondrial manganese superoxide dismutase polymorphic variant Ile58Thr reduces activity by destabilizing the tetrameric interface. *Biochemistry*, **35**, 4287-4297.
- Brunger, A. T. (1992). *X-PLOR. Version 3.1. A System for X-ray Crystallography and NMR*, Yale University Press, New Haven, CT.
- Bull, C. & Fee, J. (1985). Steady-state kinetic studies of superoxide dismutases: properties of the iron containing protein from *Escherichia coli*. *J. Am. Chem. Soc.* **107**, 3295-3304.
- Edwards, R. A., Whittaker, M. M., Whittaker, J. W., Jameson, G. B. & Baker, E. N. (1998a). Distinct

- metal environment in Fe-substituted manganese superoxide dismutase provides a structural basis of metal specificity. *J. Am. Chem. Soc.* **120**, 9684-9685.
- Edwards, R. A., Baker, H. M., Whittaker, M. M., Whittaker, J. W., Jameson, G. B. & Baker, E. N. (1998b). Crystal structure of *Escherichia coli* manganese superoxide dismutase at 2.1 Å resolution. *J. Biol. Inorg. Chem.* **3**, 161-171.
- Genick, U. K., Soltis, S. M., Kuhn, P., Canestrelli, I. L. & Getzoff, E. D. (1998). Structure at 0.85 Å resolution of an early protein photocycle intermediate. *Nature*, **392**, 206-209.
- Guan, Y., Hickey, M. J., Borgstahl, G. E. O., Hallewell, R. A., Lepock, J. R., O'Connor, D., Hsieh, Y., Nick, H. S., Silverman, D. N. & Tainer, J. A. (1998). Crystal structure of Y34F mutant human mitochondrial manganese superoxide dismutase and the functional role of tyrosine 34. *Biochemistry*, **37**, 4722-4730.
- Holm, R. K., Kenepohl, P. & Solomon, E. I. (1996). Structural and functional aspects of metal sites in biology. *Chem. Rev.* **96**, 2239-2314.
- Hopkin, K. A., Papazian, M. A. & Steinman, H. M. (1992). Functional differences between manganese and iron superoxide dismutases in *Escherichia coli* K-12. *J. Biol. Chem.* **267**, 24253-24258.
- Hsieh, Y., Guan, Y., Tu, C., Bratt, P. J., Angerhofer, A., Lepock, J. R., Hickey, M. J., Tainer, J. A., Nick, H. S. & Silverman, D. N. (1998). Probing the active site of human manganese superoxide dismutase: the role of glutamine 143. *Biochemistry*, **37**, 4731-4739.
- Keele, B. B., McCord, J. M. & Fridovich, I. (1970). Superoxide dismutase from *Escherichia coli* B. *J. Biol. Chem.* **245**, 6176-6181.
- Lah, M. S., Dixon, M. M., Patridge, K. A., Stallings, W. C., Fee, J. A. & Ludwig, M. L. (1995). Structure-function in *Escherichia coli* Iron superoxide dismutase; comparisons with the manganese enzyme from *Thermus thermophilus*. *Biochemistry*, **34**, 1646-1660.
- Laskowski, R. A., MacArthur, M. W., Moss, D. S. & Thornton, J. M. (1993). PROCHECK: a program to check the stereochemical quality of protein structures. *J. Appl. Crystallog.* **26**, 283-291.
- Leslie, A. G. W. (1990). *Macromolecular Data Processing*, Oxford University Press, Oxford.
- Ludwig, M. L., Metzger, A. L., Patridge, K. A. & Stallings, W. C. (1991). Manganese superoxide dismutase from *Thermus thermophilus* a structural model refined at 1.8 Å resolution. *J. Mol. Biol.* **219**, 335-358.
- Matthews, B. W. (1968). Solvent content in protein crystals. *J. Mol. Biol.* **33**, 491-497.
- Schlichting, I., Berendzen, J., Jr, G., N. P. & Sweet, R. M. (1994). Crystal structure of photolysed carbonmonoxy myoglobin. *Nature*, **371**, 808-812.
- Schmidt, M. (1999). Manipulating the coordination number of the ferric iron within the cambialistic superoxide dismutase of *Propionibacterium shermanii* by changing the pH-value. A crystallographic analysis. *Eur. J. Biochem.* **262**, 117-126.
- Steinman, H. M. (1992). Construction of an *Escherichia coli* K-12 strain deleted for manganese and iron superoxide dismutase genes and its use in cloning the iron superoxide dismutase gene of *Legionella pneumophila*. *Mol. Gen. Genet.* **232**, 427-430.
- Tierney, D. L., Fee, J. A., Ludwig, M. L. & Penner-Hahn, J. E. (1995). X-ray absorption spectroscopy of the iron site in *Escherichia coli* Fe(III) superoxide dismutase. *Biochemistry*, **34**, 1661-1668.
- Whittaker, J. W. & Whittaker, M. M. (1991). Active site spectral studies on manganese superoxide dismutase. *J. Am. Chem. Soc.* **113**, 5528-5540.
- Whittaker, M. M. & Whittaker, J. W. (1996). Low-temperature thermochromism marks a change in coordination for the metal ion in manganese superoxide dismutase. **35**, 6762-6770.
- Whittaker, M. M., Ekberg, C. A., Edwards, R. A., Baker, E. N., Jameson, G. B. & Whittaker, J. W. (1998). Single crystal polarized spectroscopy of manganese superoxide dismutase and electronic structure of the active site metal complex. *J. Phys. Chem. B*, **102**, 4668-4677.

Edited by R. Huber

(Received 12 October 1999; received in revised form 28 December 1999; accepted 28 December 1999)